Chemical Engineering Journal 164 (2010) 121–131

Contents lists available at ScienceDirect

Chemical Engineering Journal

journal homepage: www.elsevier.com/locate/cej

Liquid flow on a vertical wire in a countercurrent gas flow

J. Grünig*, T. Skale, M. Kraume

Chair of Chemical and Process Engineering, Technische Universität Berlin, Straße des 17. Juni 135, D-10623 Berlin, Germany

ARTICLE INFO

Article history:
Received 2 March 2010
Received in revised form 2 August 2010
Accepted 17 August 2010

Keywords:
Wetted wire packing
Falling film
Film thickness
Interfacial area
Specific pressure drop

ABSTRACT

The concept of the wire bundle packing is regarded as a potential alternative to common structured packings in the chemical industry, but until now it is still in prototype stadium and its capability has to be proven. The packing mainly consists of parallel vertical wires that are supplied with liquid separately from a special liquid distributor. To gain insight into the fluid dynamics of the gas/liquid flow, experiments with a single wire in a channel are conducted. Different methods are employed to measure local film thicknesses, liquid hold-up, liquid bead velocities, load limits and pressure drop. Due to the strongly curved surface of the wire, the film flow differs from the fluid dynamics of liquid films on plane surfaces. The film flow shows a distinctive pattern of liquid "beads" that run on a thin basis film. When the film is subject to a significant counter current gas flow the flow pattern changes, but the liquid hold-up and the interfacial area are hardly influenced. This behaviour can be observed up to the load limit where the beads disintegrate and flooding occurs. An estimation of the fluid dynamic performance of the wire packing from the single wire experimental data is made. The results indicate that the interfacial area of the fully wetted packing exceeds the dry packing area up to 60%. The estimated pressure drop is about one magnitude lower than that of a comparable corrugated sheet structured packing and the load limits are significantly higher.

1. Introduction

Liquid films are widely used in apparatuses for heat and mass transfer in gas–liquid systems. In packed columns for distillation or absorption, the liquid is distributed on the surface of internal packings to provide a large interfacial area for heat and mass transfer. Today, the most widely used structured packings in the industry are cross corrugated sheet packings which were developed in the 1960s. They offer low specific pressure drop and high separation efficiencies and are easy to manufacture. Their structure provides inclined gas passages that cause intensive radial mixing of the gas phase and an increase of the local gas velocity. In spite of all the advantages, uniform liquid distribution in the packing is still a problem. This is of importance since maldistribution reduces the separation efficiency significantly.

An alternative packing concept which consists of bundles of vertical wires is expected to solve the problem of liquid distribution. Liquid is supplied to each single wire by a special liquid distributor and flows down on it as annular film. By this means a very uniform radial liquid distribution over the whole packing height can be achieved provided that the uniformity of the initial liquid distribution is ensured. This is crucial since the packing has no self-distribution properties. Compared to corrugated sheet packings, the paths for gas flow are straight. This reduces the effective gas velocity and the abrupt direction changes of the gas flow inside the packing. As a result, the specific pressure drop decreases and the load limits increase. This effect can also be found when comparing corrugated sheet packings with different corrugation angles.

But until now, the wetted wire concept is in experimental stage and only few prototypes on lab scale have been built. There are technical problems that still have to be solved for the use in practical applications such as the liquid distribution and the installation of the packing in the column. And the most important is if the advantageous fluid dynamic behaviour goes along with reasonable separation efficiency.

This work focuses on the fluid dynamics of the liquid film on a single wire. One the one hand, one gets a detailed view on the film flow how it appears in the packing. On the other hand, it allows estimating the fluid dynamic performance of the wire packing. But to draw a conclusion if the packing is eventually feasible, mass transfer measurements have to be performed as well.

The vast majority of investigations on falling liquid films are made on planar surfaces, whereas curved surfaces are considered planar when the film thickness is comparatively small to the radius of the curvature. To avoid boundary effects, most experiments were performed at the inner and outer walls of tubes. The first theoretical description of falling film flow in the laminar regime was given

* Corresponding author at: Ackerstraße 71-76, D-13355 Berlin, Germany.
Tel.: +49 30 314 72687; fax: +49 30 314 72756.
E-mail address: jochen.gruenig@tu-berlin.de (J. Grünig).

1385-8947/$ – see front matter © 2010 Elsevier B.V. All rights reserved.
doi:10.1016/j.cej.2010.08.040

by Nusselt [1]. With the assumption of a developed velocity profile, the theoretical film thickness can be calculated. Several authors presented empirical equations based on experimental data for the different flow regimes from laminar to fully turbulent flow [2–6]. It showed that even in a pseudo-laminar regime the mean film thickness of the wavy film is equal to the theoretical Nusselt solution. In the fully turbulent region the flow shows irregular wave patterns and the mean film thickness deviates from the Nusselt solution. Further investigations on the wavy structure of the turbulent film were conducted e.g. by Portalski and Clegg [7], Chu and Dukler [8] and Takahama and Kato [9].

When considering a film on a highly curved surface, such as a wire, where the radius of curvature of the wetted surface is in the order of magnitude of the film thickness the film flow can no longer be described by the equations for planar liquid films. Grabbert and Wünsch [10] made a theoretical comparison between laminar films on curved and planar surfaces and showed the influence of the curvature on the fluid dynamics. When comparing laminar films of the same film thickness, an increase in curvature causes higher velocities and a steeper velocity profile. Besides this, the curvature promotes the formation of waves due to the instability caused by influence of the surface tension which was first theoretically described by Rayleigh [11]. This phenomenon leads also to the disintegration of liquid jets as described by Weber [12]. There are several studies focusing on the instabilities of films on wires or fibres since it has also a technical relevance for coating processes. Goren [13] made a theoretical and experimental study for creeping flow of thin liquid films on wires. He chose the liquid viscosities and surface tension so high and the radius of the wire so small that the gravitational forces could be neglected compared to viscous and surface forces. He found that for a given parameter set there is a disturbance of a certain wavelength which grows faster than disturbances of other wavelengths. This leads to the formation of capillary waves that appear as “beads” with a distance which is given by this wavelength. Lin and Liu [14] made similar studies for falling films on a wire and taking also the gravitational forces into account. They found that the film is practically instable for all values of the liquid Reynolds number and the ratio of film and wire radii. Trifonov [15] calculated wavy regimes of viscous liquid films on wires. The results showed a significant influence of the curvature on the wave formation. Experiments by Quéré [16] showed that a mean flow can lead to beads of constant amplitude and prevent the break-up of the film. Recent works that include numerical simulations and experiments distinguish different flow regimes [17–22]. For low flow rates and thin wires, a primary instability forms evenly spaced beads which maintain uniform shape over the whole length of the wire. At larger flow rates and thicker wires the flow becomes irregular after a certain height. Due to coalescence processes, large beads are formed which are running down with higher velocity and swallow smaller slow-moving beads. There remains a thin smooth basis film in their wake which again can form visible beads. As simulations revealed, inner circulation can occur in large beads so they act like roll waves which transport mass by their motion.

An idea to use this special form of liquid films for technical purposes was proposed by Hattori et al. [23]. They suggested a wire packing for heat and mass transfer processes and made single wire experiments. Further experiments on fluid dynamics and mass transfer of films on single wires were performed by Chinju et al. [24] and Uchiyama et al. [25]. Migita et al. [26] built a prototype wetted wire column with an inner diameter of 70 mm and a packing consisting of 109 parallel wires. They performed desorption experiments with CO_2/N_2 gas mixtures into aqueous monoethanolamine solution (MEA) and also measured the specific pressure drop. It appeared that the separation efficiency is comparable to common packings but the specific pressure drop is about one magnitude lower. This would make the wire packing suitable for applications where a low pressure drop is important like e.g. vacuum distillation or flue gas cleaning.

Most publications dealing with cylindrical film flow do not consider the interaction of the film flow with a counter current gas phase as it occurs in a packed column. In the work of Migita et al. [26] the gas velocities are low enough that there is practically no influence on the film fluid dynamics. Our work focuses on the two-phase flow of annular falling films at higher gas loads where there film flow is affected by the counter current gas flow. The aim of this investigation is to estimate the performance of the fluid dynamics of a wetted wire packing at higher gas loads ($F_P > 3\ Pa^{0.5}$).

2. Materials and methods

2.1. Experimental setup

The flow sheet of the experimental setup is shown in Fig. 1. The main element is a vertical channel with a centrically fixed wire. Liquid is pumped from a storage tank (0.5 L flask) to the top of the channel by a gear type pump (BVP-Z 186, Ismatec GmbH, Germany). A check valve is installed to avoid the back-flow of the liquid while the pump is switched off. To adjust the liquid temperature, a heater is installed. The liquid is supplied to the wire inside the channel head and runs down as liquid film and gets into contact with the gas phase. At the channel bottom, the liquid is caught by a collector tube and fed back into the storage tank. The collector tube and the storage tank are connected by flexible hoses and a pressure equalization line (not shown in Fig. 1) in such a way that they share the same liquid level. The weight of the storage tank is measured with an electronic balance (BL 1500 S, Sartorius AG, Germany) to detect changes of the circulating liquid mass due to evaporation inside the channel. Any amount of liquid which is possibly thrown against the channel walls misses the collector tube and is drained off separately.

The air is taken from the domestic compressed air net which is filtered and decompressed to system pressure (up to 5 mbar above ambient pressure) which is measured by a U-tube manometer. A temperature controlled electrical heater (LHS System 20 S, Leister, Switzerland) of 1 kW power heats the air to the desired temperature before it is guided into the bottom of the channel. To reduce heat losses the airflow is insulated. After having passed through the channel the air leaves at the top into the environment. To prevent liquid droplets from being discharged into the environment, a phase separator has been installed in the exhaust air path.

Fig. 2 shows details of the channel's head and bottom section. The channel is made of four glued glass sheets of 4 mm wall thickness and has a quadratic free cross section of 20 mm × 20 mm and a length of 1 m. The wire is made of stainless steel with a diameter of 1 mm and an untreated surface of technical roughness which is carefully cleaned with acetone. It is fixed at the bottom, tightened by a stretching device at the head and sealed at both sides. The head body is made of acrylic glass and holds a brass insert with a liquid feed tube of stainless steel with an inner diameter of 2 mm. With an adjustment mechanism it is possible to limit the excentricity of the annular gap between the wire and the feed tube to ±0.1 mm to achieve a uniform initial liquid distribution. The bottom section contains a liquid collector glass tube (ID ø 8 mm). The lower part of the liquid collector is made of Teflon and has ø 8 mm hose connections for the liquid outlets. Air is guided into the bottom chamber via four inlet ports which are placed in the mounting plate. An intake guide is mounted at the entrance of the channel to ensure a smooth transition of the gas flow.

The liquid flow rate is governed by the calibrated rotary frequency of the gear pump in a range from 10 mL/min to 90 mL/min (corresponding to a liquid load of $B_W = 0.2 \ldots 1.7\ m^3/(m\,h)$, rela-

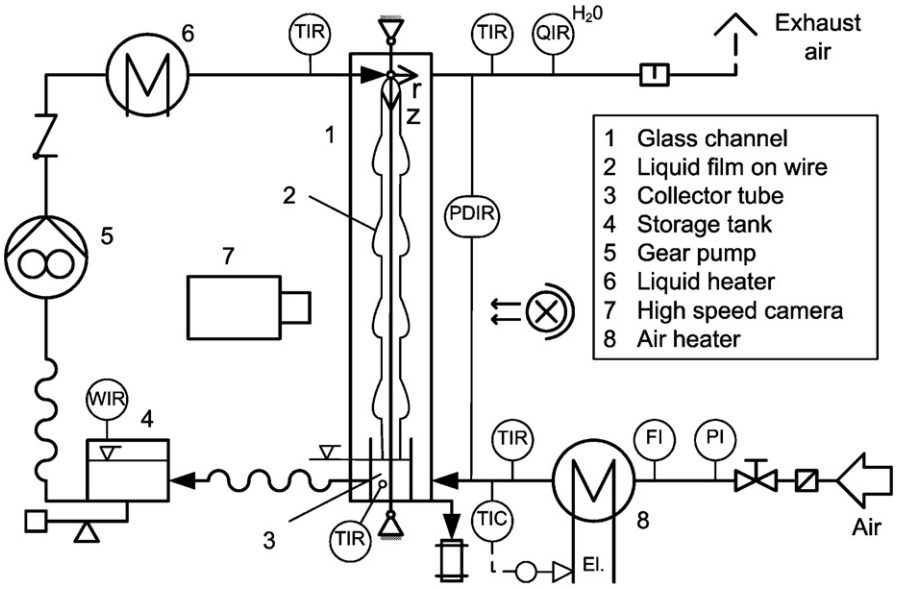

Fig. 1. Sketch of experimental setup.

tive uncertainty ±2%). Gas flow rates are adjusted with a throttle valve and measured by a flow meter between 0 m^3/h and 10 m^3/h (corresponding to a gas load of $F_C = 0...7.6\ Pa^{0.5}$, relative uncertainty ±6%). Temperatures are controlled to have the same value at the inlet of each phase and varied from room temperature to 70 °C.

A digital CMOS high-speed camera (MV-D752-160, Photonfocus AG, Switzerland) combined with a synchronized pulsed back lighting (LED element: 300 mm × 18 mm, LND-330A-DF, CCS Inc.; LED lighting controller: PP602, Gardasoft Vision Ltd.) is used for shadowgraphy measurements of the film flow. The camera has a maximum frame rate of 340 fps at a spatial resolution of 752 × 582 pixels. It is possible to reduce the region of interest of the image sensor to increase the frame rate. A telecentric lens (S5LPJ0420, Sill Optics GmbH), which delivers magnified undistorted pictures, is used for film thickness measurements. For the detection of the bead velocity, a wide-angle lens (Pentax 12 mm TV lens) is employed. The camera is mounted on a carriage to adjust the focal plane to the wire axis. Furthermore, the vertical position of the camera and the lighting can be varied. The channel inlet and outlet temperatures of liquid and gas are measured by thermocouple sensors (Type K, Newport GmbH). To measure the pressure loss over the length of the channel, a differential pressure transducer of precision U-tube type (Betz GmbH) is installed between the gas in- and outlet.

To examine the influence of physical properties, different liquids were used. Deionised water was taken from an ion-exchange purifying system. Ethanol (Merck KGaA, Germany) of synthesis grade with a purity of 99.5% was used. Paraffin oil was used as received from the supplier (Fauth & CO. KG, Germany); the viscosity was measured with a rotational viscometer (Anton Paar Rheolab QC, Haake VT 550) and the surface tension with a pendant drop type tensiometer. An overview of the physical properties of the liquids is given in Table 1.

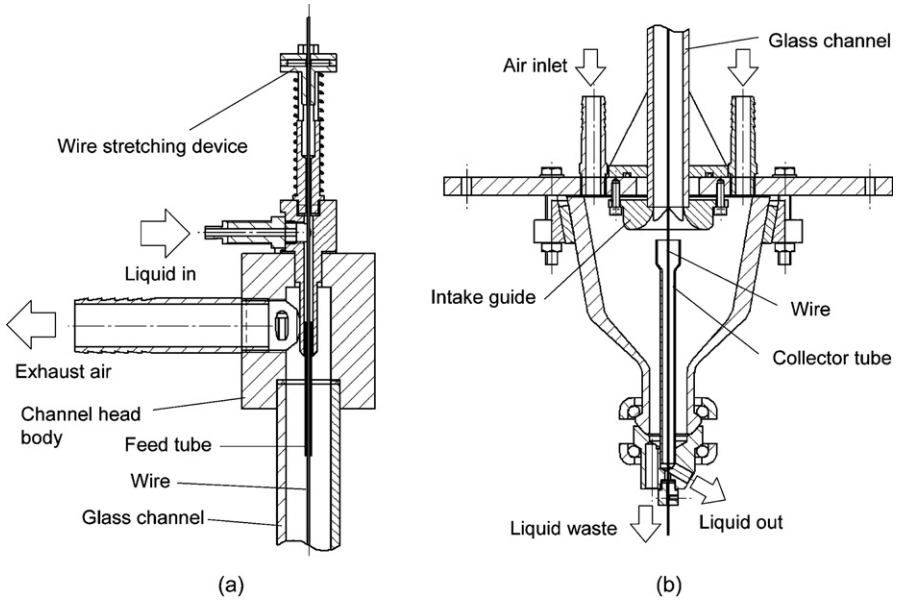

Fig. 2. Cross section of channel head.

Table 1
Physical properties of the tested liquids at 20 °C.

	ρ [kg/m^3]	η [mPa·s]	σ [mN/m]
Water	998[a]	1.0[a]	72.7[b]
Ethanol	790[a]	1.2[a]	22.3[b]
Paraffin oil	830[c]	16.0[c]	28.3[c]

[a] [28].
[b] [27].
[c] Own measurements.

2.2. Film thickness measurements

Due to the good optical accessibility of the channel and the absence of optical distortions, the non-intrusive shadowgraphy method is used to detect the film thickness. The transparent liquid film is identified by its boundary, which appears as dark shadow on the images. To get a local time-dependent thickness profile with high temporal resolution, only a narrow region of 20 × 752 pixels was chosen. This allowed recording image sequences with a frame rate of f_R = 1000 fps and a recording time of t_R = 5 s or 10 s. The sequences were analyzed by image processing software (Image-Pro Plus 5.1, Media Cybernetics Inc.). The diameter of the dry wire was used as calibration length to convert the pixels into length information with an accuracy of ±10 μm, resulting in a relative uncertainty of the film thickness of ±10% at δ = 100 μm and ±1% at δ = 1500 μm. To handle the large amount of data, a macro was written which automatically exports the results into MS Excel sheets. Fig. 3 shows an example of a film thickness profile. One can easily distinguish the beads, appearing as sharp peaks, and the basis film. For the automatic recognition of the beads a threshold value of δ = 500 μm was introduced which turned out to be valid over the whole parameter range since it was observed that the basis film never reaches this value. An overstepping of the threshold is regarded as the appearance of a bead and the peak height is taken as bead thickness. The basis film thickness was counted when the deviation from the mean value was lower than 5% over a period of 0.02 s. From these data, mean values of the bead thickness, bead frequency and basis film thickness were determined which were time-averaged over the recording time.

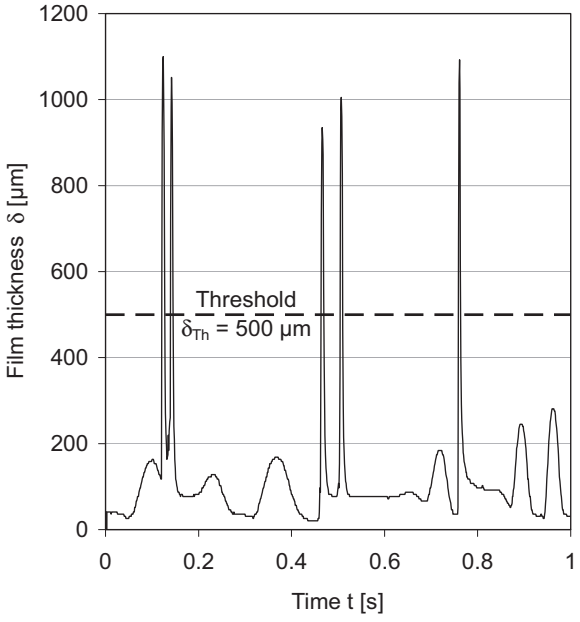

Fig. 3. Example of film thickness profile recording.

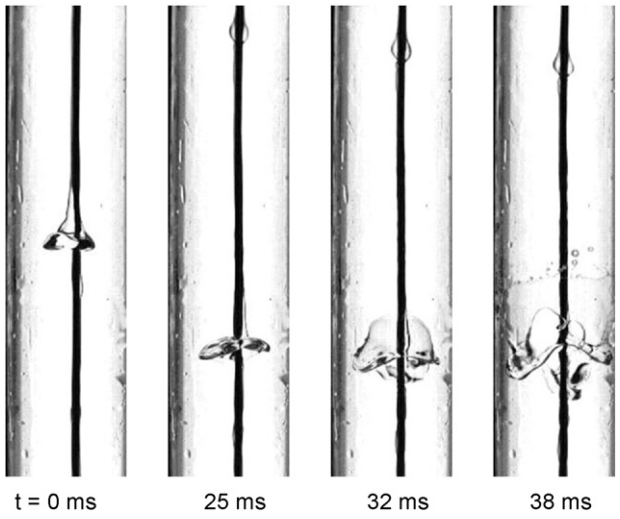

Fig. 4. Sequence of the breakage of an ethanol bead.

2.3. Liquid hold-up measurements

As can be seen in Fig. 1, the collector tube and the storage tank are interconnected and thus have the same liquid level. When the pump is switched off, the remaining liquid film on the wire drains into the collector tube and causes a strong increase in the weight of the storage tank which is recorded by the electronic balance. The additional liquid volume in the collector tube caused by the level rising is not detected by the balance. Therefore it is estimated by means of the liquid surface area ratio of storage tank and sample tube. The step response is characterized by a steep rise in the beginning which is caused by fast draining beads of the mass ΔM_B. Thereafter, the remaining basis film drains and causes a slow rise of the curve until the film is ripped up and the drainage is stopped. A small amount of liquid remains at the wire in the form of adherent drops in the range of few microliters.

The averaged value of ten jumps gives a mean liquid mass on the wire that is converted to a mean liquid hold-up $HU_l = \Delta M_{tot}/(\rho_l \cdot L_W)$ which is referred to the length of the wire (relative uncertainty ±8%). This quantity can be interpreted as the mean cross-sectional area of the film.

2.4. Load limit measurements

The load limits are identified by visual observation. At a certain gas load some of the largest beads start to break up into small droplets which are entrained by the gas flow (see Fig. 4). Thus, this point is regarded as the onset of entrainment. A further increase of the gas load causes the flooding of the channel which is characterized by the complete retention of the liquid. The phenomenon of bead breakage is more pronounced in the case of ethanol while the bead breakage of water leads directly to the flooding of the channel.

2.5. Bead velocity measurements

The bead velocity is observed with the high-speed camera equipped with the wide-angle lens. The image size covers about 12 cm of the channel height. A scale which is attached to the channel serves as calibration length. To analyze the image sequences, the same image recognition software is used as for the film thickness measurements. In order to detect the beads as discrete objects and distinguish those from the basis film areas of interest are arranged in the images on each side of the wire. By this means, only the bead crests which extend into these areas are recognized. A track-

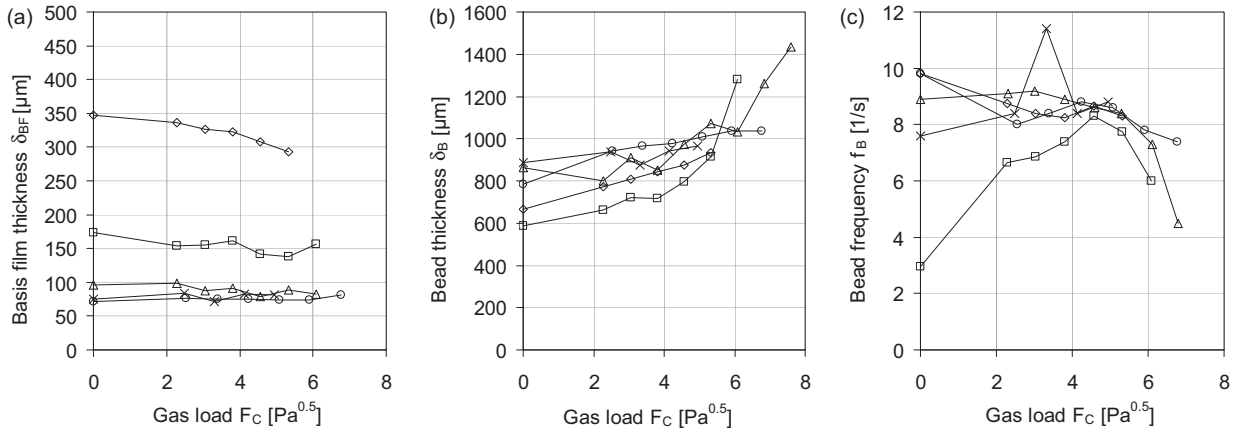

Fig. 5. Basis film thickness (a), bead thickness (b) and bead frequency (c) depending on the gas load for different liquid properties. Liquid and temperature: ◊ paraffin oil 20 °C, □ ethanol 20 °C, △ water 20 °C, × water 40 °C, ◯ water 60 °C; B_W = 0.2 m³/(m h), z = 730 mm.

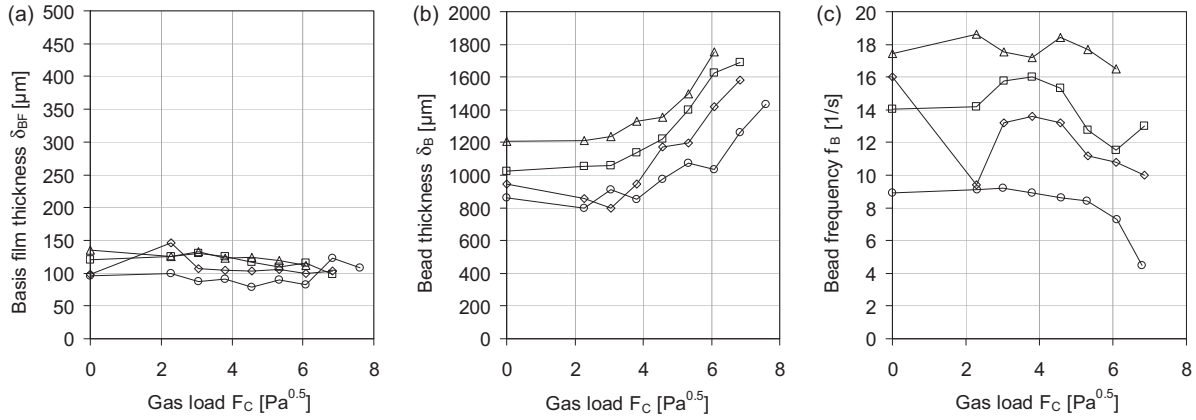

Fig. 6. Basis film thickness (a), bead thickness (b) and bead frequency (c) depending on the gas load for different liquid loads B_W = ◯ 0.2, ◊ 0.6, □ 1.0, △ 1.7 m³/(m h); water, T = 20 °C, z = 730 mm.

ing function of the program is used to follow the path of the beads as they move downwards. The relative uncertainty of this measurement method is ±5%.

2.6. Pressure drop measurements

The measured pressure drop is mainly caused by friction of the channel walls and the additional channel inlet and outlet resistances (relative uncertainty ±2%). Anyhow, there is an observable rise in the pressure drop when the wire is loaded with liquid (up to 10 Pa). When dividing the definition equations for the friction factor for wetted and dry condition (Appendix B), the increase of the friction factor due to the counter current film flow can be calculated:

$$\frac{\zeta_{l,C}}{\zeta_C} = \frac{\Delta p_{l,C}}{\Delta p_C}(1 - h_{l,C})^2 \frac{d_{hl,C}}{d_{h,C}}. \quad (1)$$

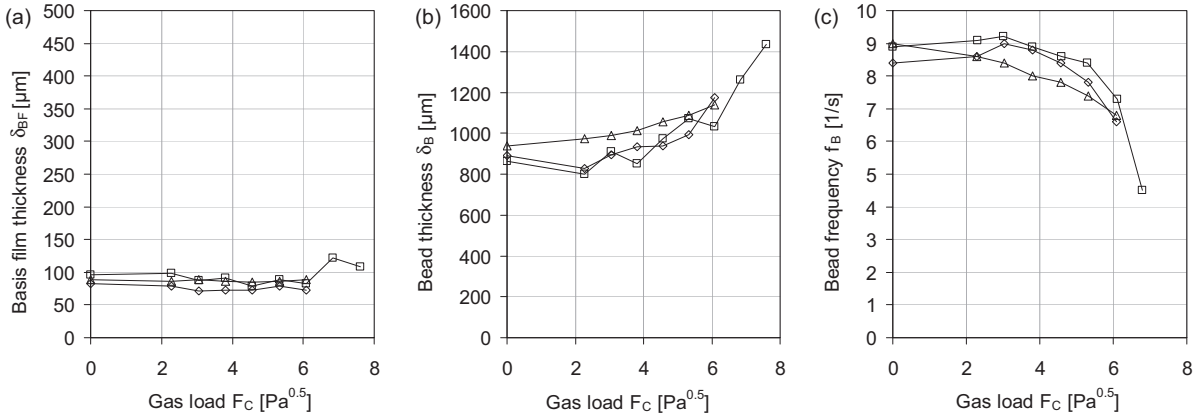

Fig. 7. Basis film thickness (a), bead thickness (b) and bead frequency (c) depending on the gas load at different vertical positions z = △ 130, ◊ 330, □ 730 mm; water, B_W = 0.2 m³/(m h), T = 20 °C.

3. Results and discussion

3.1. Film thickness

In the measured liquid load range, the film flow shows an irregular pattern of beads of different sizes. Therefore, the film thickness data was averaged over the recording time. The results of the film thickness measurements are shown in Figs. 5–7. The mean basis film thickness, mean bead thickness and mean bead frequency are plotted against the gas load F_C. The plots are showing the variation of the liquid properties, the liquid load B_W and the running length z of the film. When considering the influence of the gas load, common phenomena can be observed for all parameter variations:

- The basis film thickness shows almost no influence of the gas load.
- The bead thickness is increased significantly with rising gas load.
- The bead frequency is reduced at high gas loads.

Comparison of different liquid properties (Fig. 5)

The basis film thickness shows a significant influence of the liquid properties. Due to higher viscosity, paraffin oil shows a higher basis film thickness than water at different temperatures. Interestingly, the variation of the temperature of water does not have a clear effect on the basis film thickness. The water film shows the largest bead thicknesses, which is assumed to be caused by its large surface tension compared to ethanol and paraffin oil. For ethanol, there is a maximum value at medium gas load. The reduced frequency at low gas loads is caused by a drippy liquid flow from the nozzle which is changed into a smooth flow at higher gas loads. In summary it can be concluded that a higher viscosity of the liquid causes a thicker basis film and at higher surface tensions the film tends to form larger beads.

Comparison of different liquid loads (Fig. 6)

An increase of the liquid load leads to slightly larger basis film thicknesses, whereas the bead thickness is clearly enhanced. Moreover, the bead frequency rises considerably with increasing liquid load. This means that at higher liquid loads a greater portion of the liquid is transported by the beads. Anyhow, a clear distinction between basis film and beads cannot be made as Chinju et al. [24] already stated. When regarding numerical results from Duprat et al. [21] of the internal streamlines for the regular bead flow on a wire, large recirculation zones appear inside a bead at higher liquid loads in which liquid volume is trapped and transported as the bead runs down. The parallel streamlines of the basis film are widened underneath the recirculation zone. This can be interpreted in such a way that the basis film is accelerated as the bead runs over it (the bead then only consists of the recirculation zone). When regarding the bead at large, it can be interpreted that the basis film enters the bead and leaves it after a certain residence time while there is no exchange with the liquid volume of the recirculation zone. For the irregular bead flow the internal flow is more complicated and it is assumed that the recirculation zone holds a significant potion of the drop volume and thus most of the liquid volume is transported inside these recirculation zones.

Chinju et al. [24] and Uchiyama et al. [25] reported that the bead size does not increase with rising liquid load. Furthermore, they measured smaller bead sizes but higher bead frequencies than in the present study. The main difference is that they measured at lower liquid loads which resulted in a regular bead pattern, whereas in this study the liquid loads where higher than the critical value at which an irregular bead pattern arises. One can conclude that in the regular flow regime an increasing liquid flow rate leads to a higher density of equally sized beads on the wire. At higher liquid load the flow becomes irregular and the faster beads swallow the slower ones which results in an increase of the mean bead thickness but also in lower bead densities.

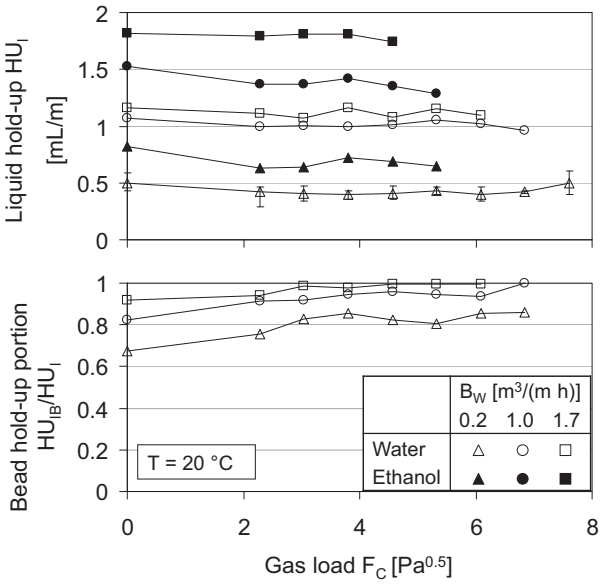

Fig. 8. Liquid hold-up and portion of the bead hold-up.

Influence of the running length (Fig. 7)

The basis film thickness shows no significant influence of the running length at the chosen positions. The bead thickness is slightly higher at the position $z = 130$ mm whereas there is no apparent difference between the values at 330 mm and 730 mm. The bead frequency is lower at 130 mm but the values at 330 mm and 730 mm also show no significant difference. This indicates that at a vertical position of 330 mm the flow structure is already fully developed and does not change further downwards.

3.2. Liquid hold-up

The liquid hold-up for water and ethanol at 20 °C in dependency of the gas load for different liquid loads is shown in the upper diagram in Fig. 8. It indicates that ethanol has a higher liquid hold-up than water. This is mainly a result of its lower density and the lower bead velocity which leads to a larger number of beads momentarily on the wire when considering similar bead frequencies. An increase of the liquid load understandably results in higher hold-up values. Remarkably, there is no increase in the liquid hold-up with increasing gas load. This behaviour is also known from packed columns at operation conditions below the load limit.

The results of the film thickness measurements revealed that the beads change their shape with increasing gas load (see Fig. 9). This affects the step response profile after liquid shut-off. With increasing gas loads there is the tendency that the steep rising edge has a greater portion on the step height. This is caused by the drainage behaviour of the beads. Apparently, when the beads are of compact shape the film drainage is completed fast. With streak-like beads the duration of the drainage is extended and the rising edge is steep in the beginning and then slowly decays to the terminal value. As a result, the liquid hold-up portion ascribed to the beads rises with increasing gas and liquid load (lower diagram in Fig. 8).

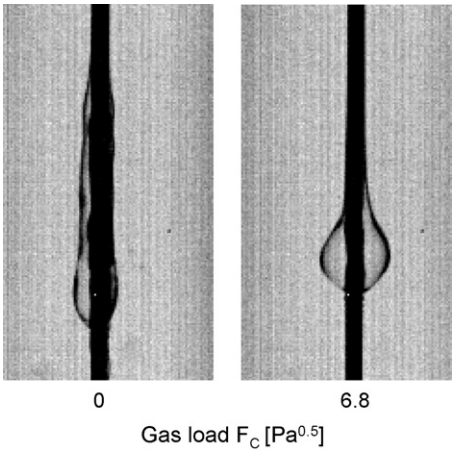

Fig. 9. Bead deformation due to counter current gas flow (ethanol, 20 °C).

The liquid hold-up can also be determined from the film thickness data with the geometric model explained in Appendix A. The mean value calculated from film thickness data from the vertical positions z = 130 mm, 330 mm and 730 mm were taken for the wire packing estimation to be consistent with the interface area calculation.

3.3. Bead velocity

The results shown in Fig. 10 indicate that there is no clear influence of the gas load on the bead velocity while a rising liquid load causes an increase in bead velocity. It turned out that the number of beads that were detected and also the resulting mean velocity depend strongly on the parameters of the tracking algorithm. The crucial parameters were the size range of the objects and the search radius, which defines the radius in which the object is searched on the following image. Since the objects often change their shape during their passage as they interfere with each other, not all of the beads can be tracked over the whole image height. In most cases, only 40% of the number of beads that were detected by the film thickness measurements could be tracked completely. This also explains the high deviation of the measurement values at high liquid loads. Since the bead velocity has only a weak influence on the value of the film surface area this can be accepted. A sensitivity analysis of the model revealed that an error of 25% in the bead velocity at $\bar{w}_B = 400$ mm/s results in a surface area deviation of 1%.

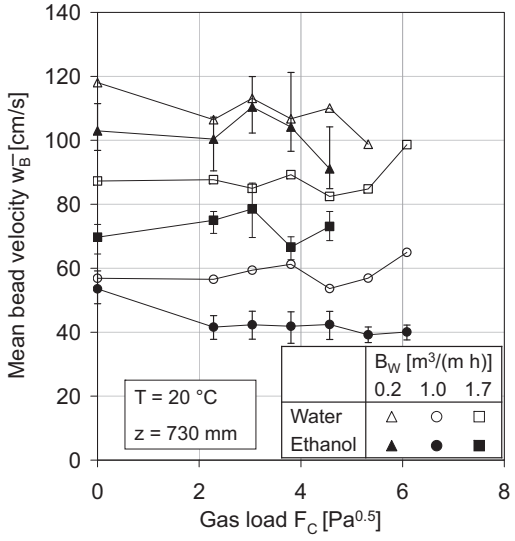

Fig. 10. Bead velocity against gas load at different liquid loads.

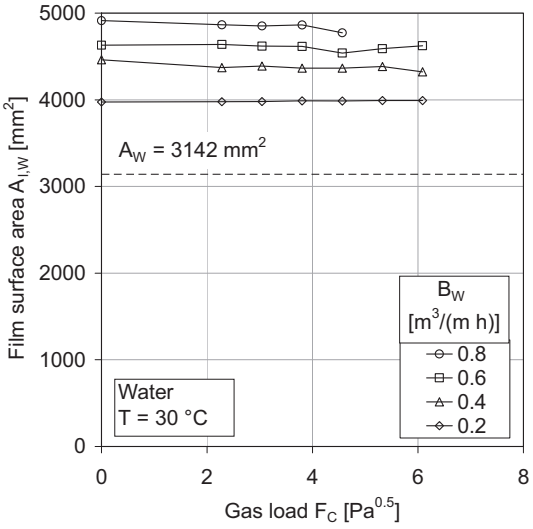

Fig. 11. Film surface area against gas load at different liquid loads.

The constant bead velocity in conjunction with a decreasing bead frequency (see Section 3.1) means that the distance between the beads increases at rising gas loads. When considering a constant liquid hold-up (see Section 3.2) over the gas load this means that the bead volume increases because the liquid volume distributes across fewer beads. This is consistent with the observation of increasing bead thickness at rising gas load. One the other hand, it was observed that the beads deform to a more compact shape what also leads to higher bead thicknesses.

3.4. Interfacial area

The model used to calculate the interfacial area is explained in Appendix A. Fig. 11 displays the calculated film surface area from film thickness data against the gas load for different liquid loads. It shows that the estimated effective film surface area is significantly higher than the surface of the dry wire A_W and rises with increasing liquid load B_W. The results indicate that the gas load has no significant influence on the film surface area. The comparison of the surface area to that of a volumetric equal liquid cylinder reveals that the surface area of the wavy film is slightly lower. It is explained by the fact that the liquid concentrates in the beads which have a lower volumetric surface area than a cylindrical annular film. This is in contrast to the plane film where waves always lead to an increase of the surface area.

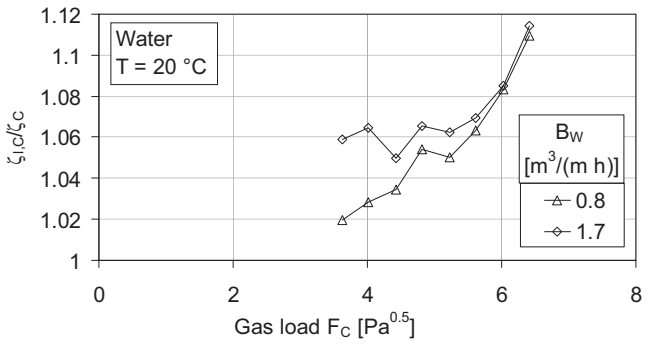

Fig. 12. Ratio of wet and dry friction factor depending on the gas loads for different liquid loads.

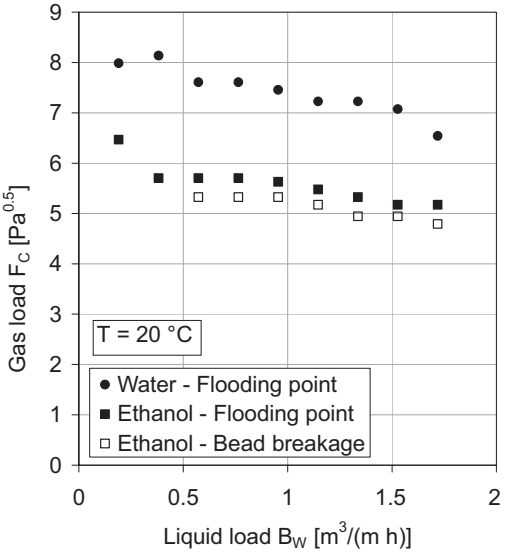

Fig. 13. Load limits of water and ethanol for the single wire.

3.5. Pressure drop

Fig. 12 shows the ratio of the wet and dry friction factor $\zeta_{l,C}/\zeta_C$ for the channel gas flow depending on the gas load F_C for two different liquid loads. It can be seen that the wet friction factor is larger at higher liquid loads which can be explained by the higher bead frequency and bead velocity. An increase of the bead velocity raises the relative velocity of the two phases and causes an additional pressure loss. Furthermore, Fig. 12 indicates an increasing wet friction factor with rising gas load. An explanation is that the deformation of the beads towards larger bead thicknesses at high gas loads leads to a larger frontal area which causes higher flow resistance.

3.6. Load limits

In Fig. 13 the gas load at bead breakage and flooding condition is plotted against the liquid load for water and ethanol. It is obvious that high load limits are reached compared to a common structured packing. However, when comparing the data with a wire packing the geometric properties have to be considered with a correction of the gas load F_C according to Eq. (21). The phenomenon of bead breakage is more pronounced in the case of ethanol while the bead breakage of water leads directly to the flooding of the channel. When increasing the gas load, the bead breakage occurs before the liquid is possibly retained. This has the effect that the portion of liquid which is thrown against the channel walls is not accounted in the hold-up measurement. Therefore, a loading point where the liquid hold-up increases with rising gas load below flooding could not be observed (see Section 3.2).

Water shows clearly higher load limits than ethanol, one reason is that the larger surface tension of water stabilizes the beads. Additionally, ethanol has a higher liquid hold-up and thus increased effective mean gas velocities at equal gas load. The minimal load limit, i.e. where the annular film is torn up and flows as a streak on one side of the wire, could not be clearly determined because the dewetting occurred spontaneously in a wide range of liquid loads below $B_W = 0.2\ m^3/(m\,h)$.

4. Estimation of wetted wire packing characteristic

To achieve high specific surface area of the packing, the wire density has to be much higher than that of the test channel. With respect to the observed maximum film thicknesses, a wire distance of 4–5 mm should be appropriate to avoid an interference of the liquid films on neighbouring wires. In Table 2 the calculated properties of wire packings with different wire densities z_P, i.e. different wire spacings in square or triangular pattern, are listed. It indicates that a wire spacing of 4 mm in square pattern and 4.3 mm in triangular pattern respectively yields a dry specific surface area of about $200\ m^2/m^3$. This is in the order of specific surface areas of common corrugated sheet packings.

Table 2
Properties of wire packings with different wire densities ($d_W = 1$ mm).

$s_{P,sq}$ [mm]	5.0	4.0	3.7
$s_{P,tri}$ [mm]	5.4	4.3	4.0
ε_P [–]	0.97	0.95	0.94
z_P [1/m^2]	40,000	62,500	72,168
a_P [m^2/m^3]	126	196	227

To adapt the results from the single wire measurements to the considered wire packing, the different voidage ε of wire packing and test channel ($\varepsilon_C = 0.998$) has to be accounted. Since the cross-sectional area for the gas flow is additionally constricted by the liquid flow, the effective mean gas velocities in the channel and the wire packing are dependent on the dry voidage ε and also the liquid fill factor h_l. For equal effective velocities in the gas passages of the channel and the wire packing the superficial gas velocities and thus the gas loads for the wire packing are less due to its lower voidage. This is accounted by a correction factor: $F_P = f_{CP} F_C$ (see Appendix B). Since both the liquid hold-up HU_l and the specific film surface area $a_{l,W}$ showed no significant dependency on the gas load below the loading point, mean values from the film thickness measurements were used for calculation.

The gas/liquid interfacial area of the packing $a_{l,P}$ is derived from the specific film surface area of a single wire $a_{l,W}$:

$$a_{l,P} = a_{l,W} \cdot z_P. \quad (2)$$

In similar manner, the specific liquid load in the packing is calculated as

$$B_P = \dot{V}_{l,W} \cdot z_P. \quad (3)$$

Fig. 14 shows the effective phase surface area of the wire packing depending on the packing liquid load for different wire densities. The specific dry packing surface is plotted in dashed lines for each wire density. It reveals that the total specific film surface of the wetted wires exceeds the value of the dry packing. Measurements on corrugated sheet packings showed that the effective surface area can also exceed the area of the geometric packing surface [29] but this is ascribed to additional effects like droplets, bubbles and ripples. Furthermore, the effective surface area rises with increasing liquid load which is mainly caused by curvature of the film surface on the single wires (see Section 3.4). Obviously, when the packing is

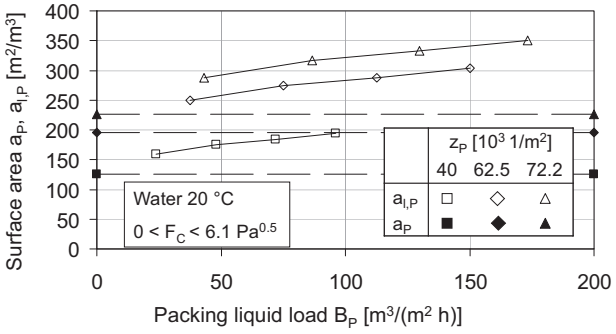

Fig. 14. Effective film surface area of the wire packing depending on the packing liquid load for different wire packing densities.

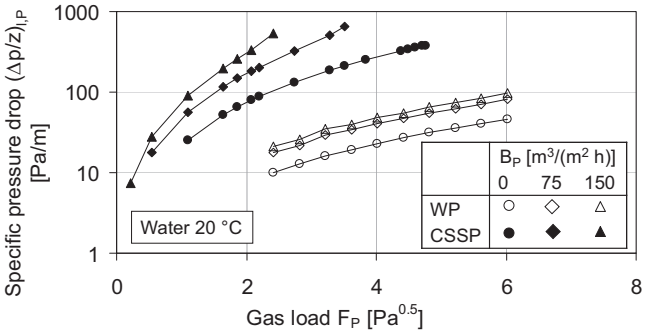

Fig. 15. Estimated specific pressure drop of the wire packing (WWP) depending on the gas load for different liquid loads compared to a corrugated sheet structured packing (CSSP).

not loaded the film surface has to be zero. It is expected that the surface area decreases significantly when the liquid load falls below a certain value due to the dewetting of the wires. This lower limit will be definitely dependent on the surface tension of the liquid and the wettability of the wire material. Since the lower liquid load limit could not accurately be specified for the single wires the behaviour of the wire packing at the lower liquid limit is still uncertain. From the observations of the dewetting of single wires can be concluded, that the dewetting process will not occur for all wires simultaneously and an abrupt decrease of the effective specific packing area is not to be expected. However, for the complete rewetting of the packing it is most likely that it is necessary to increase the liquid load above the lower load limit.

The approach for the estimation of the specific pressure drop of a wire packing is explained in the following. First, the pressure drop for turbulent flow of the dry packing is calculated by an approach of Rehme [30]:

$$\left(\frac{\Delta p}{z}\right)_{\mathrm{P}} = \zeta_{\mathrm{P}} \frac{\rho_{\mathrm{g}}}{2} \bar{w}_{\mathrm{g,P}}^2 \frac{1}{d_{\mathrm{h,P}}},$$

$$\sqrt{\left(\frac{8}{\zeta_{\mathrm{P}}}\right)} = A\left[2.5\ \ln\left(Re_{\mathrm{g}}\sqrt{\left(\frac{\zeta_{\mathrm{P}}}{8}\right)}\right) + 5.5\right] - G^*. \tag{4}$$

A and G^* are geometric factors witch depend on the wire distance and the wire diameter. For a packing with in infinite extension they are calculated as

$$A = 1,\ G^* = \frac{3.966 + 1.25x}{1+x} + 2.5\ \ln\ 2(1+x),$$

$$x = \frac{s_{\mathrm{P}}}{d_{\mathrm{W}}}\sqrt{\frac{2\sqrt{3}}{\pi}}(\text{triangular}). \tag{5}$$

With Eq. (16) the wet specific pressure drop of the packing can be estimated as

$$\left(\frac{\Delta p}{z}\right)_{\mathrm{l,P}} = \frac{\zeta_{\mathrm{l,P}}}{\zeta_{\mathrm{P}}} \frac{1}{(1-h_{\mathrm{l,P}})^2} \frac{d_{\mathrm{h,P}}}{d_{\mathrm{hl,P}}} \left(\frac{\Delta p}{z}\right)_{\mathrm{P}}. \tag{6}$$

The factor $(\zeta_{\mathrm{l,P}}/\zeta_{\mathrm{P}})$ is replaced by the ratio of friction factors $(\zeta_{\mathrm{l,C}}/\zeta_{\mathrm{C}}) = f(F_{\mathrm{C}}, B_{\mathrm{W}})$ found for the channel. Although this approach seems to be reasonable it still needs to be verified by multi-wire experiments as there might be an influence of an interaction of films on neighbouring wires. In Fig. 15 the estimated wet specific pressure drop of a wire packing with a wire density of 62,500 wires/m^2 is plotted against the gas load for different packing liquid loads. The pressure drop rises with increasing gas load while the curves for increasing liquid load are shifted toward higher pressure drop. In the considered range a loading point as observed in common packings [31] can be not identified. The loading point is reached when the gas load is high enough to increase the liquid hold-up.

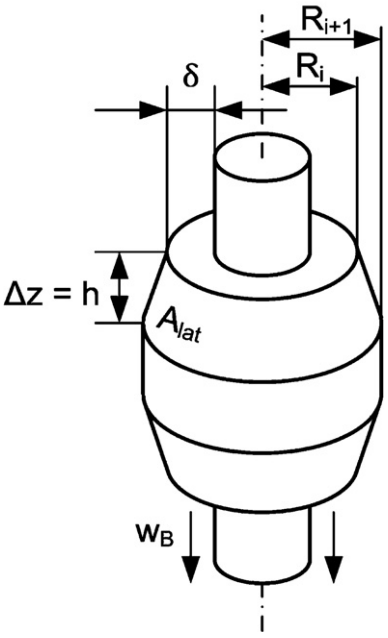

Fig. 16. Annular section model for film surface area estimation.

This causes steeper pressure drop slopes in the plot due to the restriction of the gas phase cross-sectional area. Since the single wire measurements showed no increase of the liquid hold-up at high gas loads this is also predicted for the wire packing. On the other hand, the transition region from normal operation to flooding condition cannot be derived directly from the single wire measurements. The load limit experiments on a single wire showed beads that disintegrate into small droplet at a certain gas load. It is not quite clear how this behaviour affects the hydraulic performance of the packing.

For comparison, pressure drop data of a common corrugated sheet packing of comparable specific surface area ($a_{\mathrm{P}} = 250\ \mathrm{m^2/m^3}$) which was calculated with model equations from Rocha et al. [32] is added to the diagram. The predicted pressure drop of the wire packing is about one magnitude smaller than that of the corrugated sheet packing. This is expected because the gas passages in the corrugated sheet packing have numerous direction changes and an extended length. Migita et al. [26] compared their laboratory scale wetted wire column ($z_{\mathrm{P}} = 32{,}075$ wires/m^2, $d_{\mathrm{W}} = 0.88$ mm) with a comparable packed column and also found that the pressure drop is significantly lower. However, they operated the system at very low gas loads ($v_{\mathrm{g,p}} < 0.3$ m/s) and liquid loads ($B_{\mathrm{P}} < 5\ \mathrm{m^3/(m^2\ h)}$). A low specific pressure drop is desired but cannot be used as a measure of quality alone considering that an empty column has the lowest possible specific pressure drop.

5. Conclusions

The investigations gave insights into the fluid dynamics of a wetted wire column and allowed to make a prediction about the operation characteristics. The single wire experiments showed a liquid film which is characterized by a thin basis film and large fast-moving beads. An increase of the gas load increases the bead thickness and lowers the bead frequency while the basis film thickness is hardly influenced. Nevertheless, the liquid hold-up and the bead velocity are virtually constant over the observed gas load range. This can be explained by an increase of the bead volume and the deformation of the beads from streak-like into compact shape. While the viscosity has an effect mostly on the basis film

thickness, a high surface tension promotes the formation of large beads. However, the film flow is considered to be developed after a running length of 330 mm or less. The pressure drop measurements revealed a rise in the friction factor ratio $\zeta_{l,C}/\zeta_C$ with increasing gas load which is mainly a result of increased flow resistance due to higher frontal area of the beads. Furthermore, the film surface area is always higher than the dry wire surface area but the waviness of the film does not increase the surface area such as for plane films. It revealed that the flooding point is reached at comparatively high gas loads.

When transferring the data of the single wire measurements to a wire packing the gas loads have to be corrected for an equal effective mean gas velocity in the gas passages. When wetted completely, a wire packing generates an interfacial area that always exceeds the dry surface area. The predicted specific pressure drop is about one magnitude lower than that of comparable corrugated sheet packings. The crucial question is if the separation efficiency is competitive to common packings which has to be examined in further investigations. But even if the efficiency is less, the wire packing could still be suitable for gas absorption or vacuum distillation applications where a low specific pressure drop is important and the requirements for product quality are not too high.

Notation

A, G^*, x	geometric factors of the packing, –
A	area, m^2
$a_{l,P}$	specific effective surface area of the packing, m^2/m^3
$a_{l,W}$	film surface area on wire, referred to the wire length, m^2/m
a_P	specific surface area of the dry packing, m^2/m^3
b_C	cross-sectional dimension of the channel, m
$B_w = \dot{V}_{1,w}/C_w$	liquid load of wire, referred to the wire circumference, $m^3/(m\,h)$
$B_p = \dot{V}_1/A_p$	specific liquid load in the packing, referred to cross-sectional area, $m^3/(m^2\,h)$
C_W	circumference of wire, m
d_W	diameter of wire, m
d_h	hydraulic diameter of the gas passage, m
$F = v_g \cdot \rho_g{}^{0.5}$	gas load, F-factor, $Pa^{0.5}$
$f_{CP} = F_P/F_C$	correction factor, –
f_R	frame rate, 1/s (fps)
h	segment height, m
$h_l = V_l/(\varepsilon\, V_{tot})$	liquid fill factor, –
$HU_l = V_{l,W}/L_W$	liquid hold-up, mL/m
L_W	length of wire, m
M	mass, kg
N	number of pictures in sequence
Δp	pressure drop, Pa
$(\Delta p/z)$	specific axial pressure drop, Pa/m
R	radius, m
$Re_g = \bar{w}_g d_h \rho_g/\eta_g$	Reynolds number of the gas phase, –
s_P	wire spacing in the packing, m
T	temperature, °C
t_R	recording time, s
V	volume, m^3
$\dot{V}$	volume flow rate, m^3/s
v_g	superficial gas velocity, m/s
$\bar{w}_B$	mean bead velocity, m/s
$\bar{w}_l$, W	mean film velocity on the wire, m/s
$\bar{w}_g$	mean gas velocity, m/s
z	vertical coordinate, m
z_P	packing density of wires per cross-sectional area, $1/m^2$

Greek letters

δ	film thickness, μm
ε	voidage, –
ζ	friction factor, –
η	dynamic viscosity, Pa·s
ρ	density, kg/m^3
σ	surface tension, N/m

Sub- and superscripts

B	bead
BF	basis film
C	channel
g	gas
l	liquid, wetted
P	packing
R	recording
ST	storage tank
sq	square pattern
Th	threshold
tot	total
tri	triangular pattern
W	wire
–	mean

Acknowledgement

The authors gratefully acknowledge the financial support of the Deutsche Forschungsgemeinschaft (DFG) for this work (Project no. KR 1639/13-1).

Appendix A. Film surface area estimation

The surface area of the film on the wire is estimated from the temporal local film thickness δ and the mean bead velocity $\bar{w}_B$. To account for the variation of the film profile and the bead velocity over the wire length, film thickness and bead velocity data from different vertical positions are analyzed. With the mean bead velocity, the time-dependent film thickness data is converted into a spatial film profile. With this data, axially symmetric annular sections are defined which represent the film on the wire (Fig. 16). The height h of these elements is calculated from the mean bead velocity $\bar{w}_B$ and the frame rate f_R:

$$h = \frac{\bar{w}_B}{f_R}. \tag{7}$$

Thus, the specific liquid hold-up HU_l can be calculated by summarizing the volume of the liquid elements and referring them to the distance that the beads would have covered during the recording time t_R.

$$HU_l = \frac{(\pi \cdot h/3)\sum_{i=1}^{N}(R_i^2 + R_i \cdot R_{i+1} + R_{i+1}^2 - (3/4){d_W}^2)}{\bar{w}_B \cdot t_R}. \tag{8}$$

In a similar manner, the overall film surface area is estimated by the summation of the lateral surface area of the elements (relative uncertainty ±2%).

$$A_{l,W} = L_W \frac{\sum_{i=1}^{N} \pi \cdot m \cdot (R_i + R_{i+1})}{\bar{w}_B \cdot t_R} \quad \text{with} \quad m = \sqrt{(R_i - R_{i+1})^2 + h^2}. \tag{9}$$

With this model, the mean film thickness $\delta_{l,W}$ and the mean liquid film velocity $\bar{w}_{l,W}$ can also be evaluated:

$$\bar{w}_{l,W} = \frac{\dot{V}_{l,W}}{HU_l}. \tag{10}$$

$$\bar{\delta}_{l,W} = \sqrt{\frac{HU_l}{\pi} + \left(\frac{d_W}{2}\right)^2} - \frac{d_W}{2}. \tag{11}$$

Appendix B. Adaptation of single wire measurement data for wetted wire packing characteristic prediction

B.1. Estimation of specific pressure drop in the packing

The hydraulic diameters of the gas passages in the wire packing and the channel in dry and wetted condition are calculated as

$$d_{h,P} = 4 \cdot \frac{\varepsilon_P}{C_W \cdot z_P} \quad \text{and} \quad d_{hl,P} = 4 \cdot \frac{\varepsilon_P(1-h_{l,P})}{a_{l,W} \cdot z_P}. \tag{12}$$

$$d_{h,C} = 4 \cdot \frac{{b_C}^2 \varepsilon_C}{4b_C + C_W} \quad \text{and} \quad d_{hl,C} = 4 \cdot \frac{{b_C}^2 \varepsilon_C(1-h_{l,C})}{4b_C + a_{l,W}}. \tag{13}$$

The specific pressure drop for the wire packing and the channel in dry and wetted condition are described with

$$\frac{\Delta p}{z} = \zeta \cdot \frac{\rho_g}{2} \bar{w}_g^2 \frac{1}{d_h} \quad \text{and} \quad \frac{\Delta p_l}{z} = \zeta_l \cdot \frac{\rho_g}{2} \bar{w}_{gl}^2 \frac{1}{d_{hl}}. \tag{14}$$

The effective mean gas velocity in wetted condition can be calculated as

$$\bar{w}_{g,l} = \bar{w}_g \cdot \frac{1}{1-h_l}. \tag{15}$$

This is different from the assumption from Buchanan [31] $\bar{w}_{g,l} = \bar{w}_g {d_h}^2/{d_{hl}}^2$ which is only valid for two phase flow in tubular channels. By dividing wetted and dry specific pressure drop and introducing Eq. (15) the following equation is achieved:

$$\frac{\Delta p_l}{\Delta p} = \frac{\zeta_l}{\zeta} \cdot \frac{1}{(1-h_l)^2} \cdot \frac{d_h}{d_{hl}}. \tag{16}$$

The hydraulic diameters are inserted according to Eqs. (12) for the wire packing and (13) for the channel.

B.2. Correction factor for superficial gas velocity

The mean effective gas velocities in the packing (P) and the channel (C) are dependent on the voidage ε and the liquid fill factor h_l:

$$\bar{w}_{g,C} = \frac{v_{g,C}}{\varepsilon_C(1-h_{l,C})}, \quad \bar{w}_{g,P} = \frac{v_{g,P}}{\varepsilon_P(1-h_{l,P})}. \tag{17}$$

The fill factors are calculated as

$$h_{l,C} = \frac{HU_l}{\varepsilon_C A_C} \quad \text{and} \quad h_{l,P} = \frac{HU_l}{\varepsilon_P A_P}. \tag{18}$$

A_C is the cross-sectional area of the channel and A_P is the cross-sectional area of a cell defined by the pattern of wire spacing (square or triangular):

$$A_C = {b_C}^2 \quad \text{and} \quad A_{P,sq} = {s_{P,sq}}^2, \quad A_{P,tri} = \frac{\sqrt{3}}{2} {s_{P,tri}}^2. \tag{19}$$

The wire density of the packing z_P can be calculated as

$$z_P = \frac{1}{A_P}. \tag{20}$$

Assuming equal effective gas velocities in both the channel and the wire packing, the corresponding superficial gas velocity and the gas load for the wire packing result in

$$v_{g,P} = f_{CP} \cdot v_{g,C} \quad \text{and} \quad F_P = f_{CP} \cdot F_C \quad \text{with} \quad f_{CP} = \frac{\varepsilon_P(1-h_{l,P})}{\varepsilon_C(1-h_{l,C})}. \tag{21}$$

References

[1] W. Nußelt, Die Oberflächenkondensation des Wasserdampfes (in German), Z. VDI 60 (1916) 541–546.
[2] S.J. Friedman, C.O. Miller, Liquid films in the viscous flow region, Ind. Eng. Chem. 33 (1941) 885–891.
[3] H. Brauer, Strömung und Wärmeübergang bei Rieselfilmen (in German), VDI-Forschungsheft, vol.457, VDI-Verlag, Düsseldorf, 1956.
[4] S. Ishigai, et al., Hydrodynamics and heat transfer of vertical falling liquid films (Part 1, classification of flow regimes), Bull. JSME 15 (1972) 594–602.
[5] S.V. Alekseenko, V.Y. Nakoryakov, B.G. Pokusaev, Wave formation on a vertical falling liquid film, AIChE J. 31 (1985) 1446–1460.
[6] P. Adomeit, U. Renz, Hydrodynamics of three-dimensional waves in laminar falling films, Int. J. Multiphase Flow 26 (2000) 1183–1208.
[7] S. Portalski, A.J. Clegg, An experimental study of wave inception on falling liquid films, Chem. Eng. Sci. 27 (1972) 1257–1265.
[8] K.J. Chu, A.E. Dukler, Statistical characteristics of thin, wavy films: Part II. studies of the substrate and its wave structure, AIChE J. 20 (1974) 695–706.
[9] H. Takahama, S. Kato, Longitudinal flow characteristics of vertically falling liquid films without concurrent gas flow, Int. J. Multiphase Flow 6 (1980) 203–215.
[10] G. Grabbert, G. Wünsch, Zur Hydraulik stark gekrümmter Rieselfilme (in German), Freiberger Forschungshefte A 517 (1973) 61–83.
[11] L. Rayleigh, On the instability of jets, Proc. Lond. Math. Soc. s1–10 (1878) 4–13.
[12] C. Weber, Zum Zerfall eines Flüssigkeitsstrahles (in German), Z. Angew. Math. Mech. 11 (1931) 136–154.
[13] S.L. Goren, The instability of an annular layer thread of fluid, J. Fluid Mech. 13 (1962) 309–319.
[14] S.P. Lin, W.C. Liu, Instability of film coating of wires and tubes, AIChE J. 21 (1975) 775–782.
[15] Y.Y. Trifonov, Steady-state traveling waves on the surface of a viscous liquid film falling down on vertical wires and tubes, AIChE J. 38 (1992) 821–834.
[16] D. Quéré, Thin films flowing on vertical fibers, Europhys. Lett. 13 (1990) 721–726.
[17] S. Kalliadasis, H.-C. Chang, Drop formation during coating of vertical fibres, J. Fluid Mech. 261 (1994) 135–168.
[18] I.L. Kliakhandler, S.H. Davis, S.G. Bankoff, Viscous beads on vertical fibre, J. Fluid Mech. 429 (2001) 381–390.
[19] C. Ruyer-Quil, et al., Modelling film flows down a fibre, J. Fluid Mech. 603 (2008) 431–462.
[20] C. Duprat, et al., Absolute and convective instabilities of a viscous film flowing down a vertical fiber, Phys. Rev. Lett. 98 (2007), doi:10.1103/PhysRevLett.98.244502.
[21] C. Duprat, C. Ruyer-Quil, F. Giorgiutti-Dauphine, Spatial evolution of a film flowing down a fiber, Phys. Fluids 21 (2009), doi:10.1063/1.3119811.
[22] R.V. Craster, O.K. Matar, On viscous beads flowing down a vertical fibre, J. Fluid Mech. 553 (2006) 85–105.
[23] K. Hattori, M. Ishikawa, Y.H. Mori, Strings of liquid beads for gas–liquid contact operations, AIChE J. 40 (1994) 1983–1992.
[24] H. Chinju, K. Uchiyama, Y.H. Mori, "String-of-beads" flow of liquids on vertical wires for gas absorption, AIChE J. 46 (2000) 937–945.
[25] K. Uchiyama, et al., Gas absorption into "string-of-beads" liquid flow with chemical reaction: application to carbon dioxide separation, Int. J. Heat Mass Transf. 46 (2003) 457–468.
[26] H. Migita, K. Soga, Y.H. Mori, Gas absorption in a wetted-wire column, AIChE J. 51 (2005) 2190–2198.
[27] C. Wohlfarth, B. Wohlfarth, Surface tension of pure liquids and binary liquid mixtures, in: M.D. Lechner (Ed.), Landolt-Börnstein—Group IV Physical Chemistry, vol. 16, 8th ed., Springer Verlag, Berlin, 1997.
[28] VDI-Wärmeatlas (Ed.), Berechnungsblätter für den Wärmeübergang (in German), 7th ed., VDI-Verlag, Düsseldorf, 1994.
[29] M.H. De Brito, et al., Effective mass-transfer area in a pilot-plant column equipped with structured packings and with ceramic rings, Ind. Eng. Chem. Res. 33 (1994) 647–656.
[30] K. Rehme, Simple method of predicting friction factors of turbulent-flow in non-circular channels, Int. J. Heat Mass Transf. 16 (1973) 933–950.
[31] J.E. Buchanan, Pressure gradient and liquid holdup in irrigated packed towers, Ind. Eng. Chem. Fundam. 8 (1969) 502–511.
[32] J.A. Rocha, J.L. Bravo, J.R. Fair, Distillation-columns containing structured packings—a comprehensive model for their performance. 1. Hydraulic models, Ind. Eng. Chem. Res. 32 (1993) 641–651.